PNAS
Proceedings of the National Academy of Sciences of the United States of America www.pnas.org

Supplementary Information

for

"Heterogeneity of functional groups in a metal-organic framework displays magic number ratios"

Andrew C.-H. Sue[a,b,1], Ranjan V. Mannige[c,1], Hexiang Deng[a,2], Dennis Cao[b], Cheng Wang[b,2], Felipe Gándara[a,3], J. Fraser Stoddart[b,4], Stephen Whitelam[c,4], Omar M. Yaghi[a,d,4]

[a]Department of Chemistry, University of California-Berkeley, and Lawrence Berkeley National Laboratory, Berkeley, CA 94720, U.S.A.

[b]Department of Chemistry, Northwestern University, Evanston, IL 60201, U.S.A.

[c]Molecular Foundry, Lawrence Berkeley National Laboratory, Berkeley, CA 94720, U.S.A.

[d]Kavli Energy NanoScience Institute, Berkeley, CA 94720, U.S.A.

[1]A.C.-H.S. and R.V.M. contributed equally to this work.

[2]Current address: College of Chemistry and Molecular Science, Wuhan University, Luojiashan, Wuhan, China 430080

[3]Current address: Materials Science Institute of Madrid – CSIC, Madrid 28049, Spain

[4]To whom correspondence should be addressed.

E-mail: stoddart@northwestern.edu, swhitelam@lbl.gov & yaghi@berkeley.edu

Table of Contents

Section S1 Experimental Results

S1.1 General Procedures

Chemicals were purchased from commercial vendors and used as received without further purification unless otherwise noted. ^{1}H & ^{13}C NMR Spectra were recorded on a Bruker Avance 400 MHz or Bruker Avance 500 MHz at ambient temperature, unless otherwise noted. Chemical shifts are listed in ppm on the δ scale and coupling constants are recorded in Hertz (Hz). Chemical shifts are reported in ppm relative to the signals corresponding to the residue non-deuterated solvents ($CDCl_3$: δ = 7.26 ppm, CD_3CN: δ = 1.94 ppm, CD_3SOCD_3: δ = 2.50 ppm). Powder X-ray diffraction (PXRD) data were obtained on a Bruker AXS D8 Advance diffractometer operated at 40 kV and 40 mA for CuKα, (λ =1.5406 Å) with a scan speed of 3 °/min and a step size of 0.050° in 2θ.

S1.2 Synthetic Procedures

$H_2\mathbf{L_r}$[S1] and $H_2\mathbf{L_b}$•$4PF_6$[S2] were synthesized by following procedures modified on the basis of those reported in the literature.

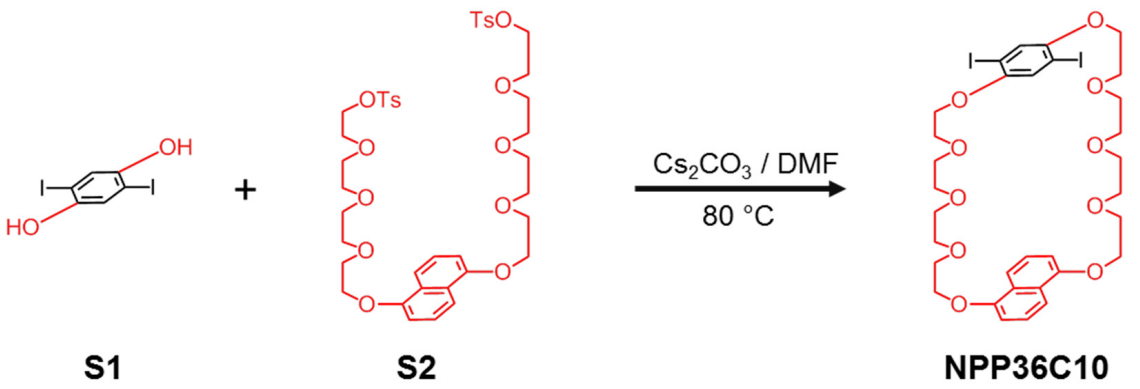

Scheme S1. Synthesis of **NPP36C10**

NPP36C10: A mixture of Cs_2CO_3 (19.1 g, 52.8 mmol) in deaerated DMF (500 mL) was heated to 90 °C under N_2. A solution of compound **S1**[S1] (5.31 g, 13.2 mmol) and **S2**[S1] (12.0 g, 13.2 mmol), dissolved in deaerated DMF (70 mL), was added to the reaction mixture using a syringe pump (1 mL / h). After 4 d, the reaction mixture was cooled to room temperature and the inorganic salts removed by filtration. The filtrate was evaporated under reduced pressure and the residue was purified by column chromatography on silica gel using CH_2Cl_2 then EtOAc / CH_2Cl_2 (3:2 v/v) to yield **NPP36C10** (3.24 g, 25%) as a microcrystalline white solid. The spectroscopic data matched that reported in the literature.[S1]

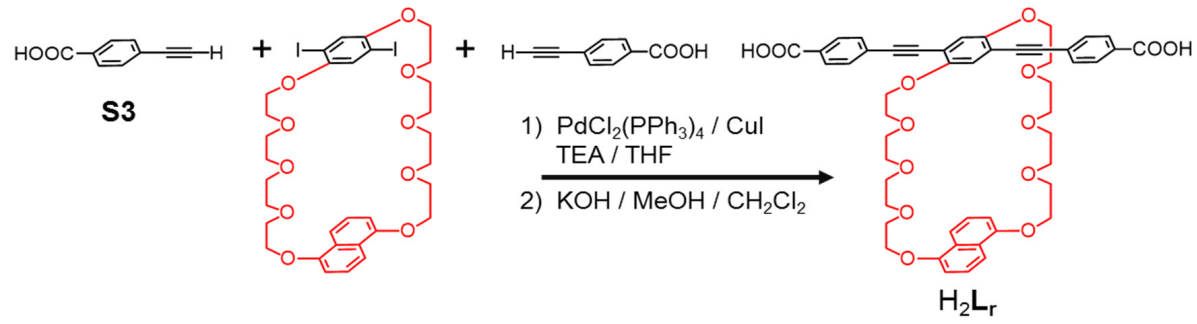

Scheme S2. Synthesis of crown ether strut $H_2\mathbf{L_r}$

$H_2\mathbf{L_r}$: A mixture of **NPP36C10** (1.50 g, 1.79 mmol), **S3**[S1] (720 mg, 4.50 mmol), $PdCl_2(PPh_3)_4$ (63 mg, 0.088 mmol), CuI (17 mg, 0.088 mmol) in a 1:2 (v/v) mixture of TEA/THF (75 mL) was heated at 85 °C for 18 h. The solvents were removed by rotary evaporation and the residue was titurated with MeOH to yield a yellow solid (1.49 g). A mixture of this yellow solid, KOH (405 mg, 7.16 mmol) and a 1:1 (v/v) mixture of CH_2Cl_2 / MeOH (25 mL) was stirred for 12 h at room temperature. The mixture was then acidified by the dropwise addition of conc HCl, precipitating $H_2\mathbf{L_r}$ (1.1 g, 70%) as a yellow solid. The spectroscopic data matched that reported in the literature.[S1]

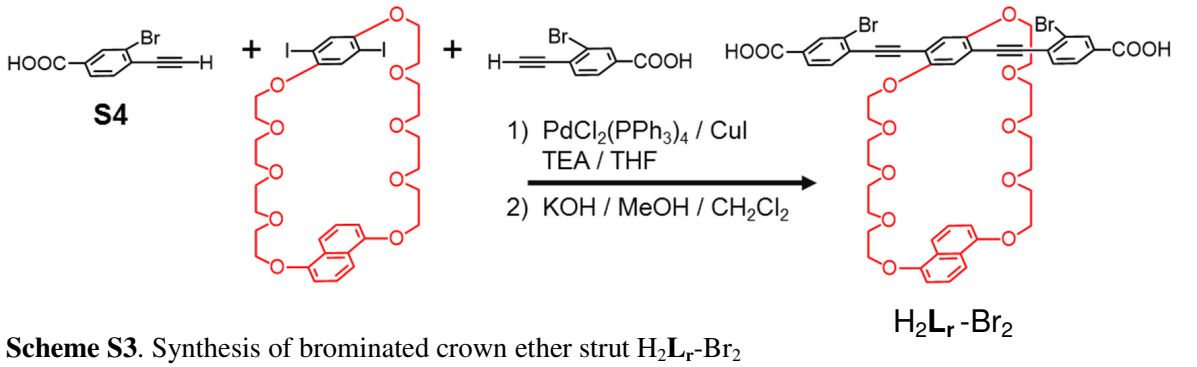

Scheme S3. Synthesis of brominated crown ether strut $H_2\mathbf{L_r}$-Br_2

$H_2\mathbf{L_r}$-Br_2: Benzoic ester **S4**[S3] (466 mg, 1.84 mmol) and **NPP36C10** (736 mg, 0.877 mmol) were dissolved in a 25/2 (v/v) mixture of THF/TEA (25 mL). $PdCl_2(PPh_3)_2$ (31 mg, 0.044 mmol) and CuI (9 mg, 0.04 mmol) were added to the solution under argon. The reaction mixture was heated under reflux for 12 h. The solvent was then removed under reduced pressure. The residue was recrystallized from MeOH. The solid material was isolated by filtration and dissolved in a 1/1 (v/v) mixture of MeOH/CH_2Cl_2 (25 mL). KOH (200 mg, 3.56 mmol) was added to the solution and the reaction mixture was left to stir for 8 h. The solvent was then removed under reduced pressure. The residue was dissolved in H_2O and filtered.

The filtrate was acidified with 6 M HCl and the resulting precipitate collected by filtration to afford $H_2\mathbf{L_r}$-Br_2 as a yellow solid (471 mg, 52%). ^{1}H NMR (CD_3SOCD_3, 500 MHz, 298 K): δ = 13.50 (s, 2H), 8.18 (d, J = 1.6 Hz, 1H), 7.96 (dd, J = 8.1, 1.6 Hz, 1H), 7.74 (d, J = 8.0 Hz, 1H), 7.63 (d, J = 8.5 Hz, 1H), 7.27 (t, J = 8.0 Hz, 1H), 7.14 (s, 1H), 6.75 (d, J = 7.7 Hz, 1H), 4.14–4.00 (m, 8H), 3.86–3.72 (m, 8H), 3.68–3.53 (m, 16H). ^{13}C NMR (CD_3SOCD_3, 125 MHz, 298 K): δ = 165.5, 153.7, 133.6, 132.8, 128.4, 125.8, 125.2, 124.3, 113.7, 112.9, 105.6, 70.2, 70.0, 70.0 70.0, 69.0, 68.8, 68.8, 67.7, 66.3; HR MS (ESI): Calcd for $C_{50}H_{48}Br_2O_{14}$ m/z = 1048.1749 $[M + NH_4]^+$, found m/z = 1048.1693 $[M + NH_4]^+$, m/z = 1030.1484 $[M + H]^+$, found m/z = 1030.1489 $[M + H]^+$.

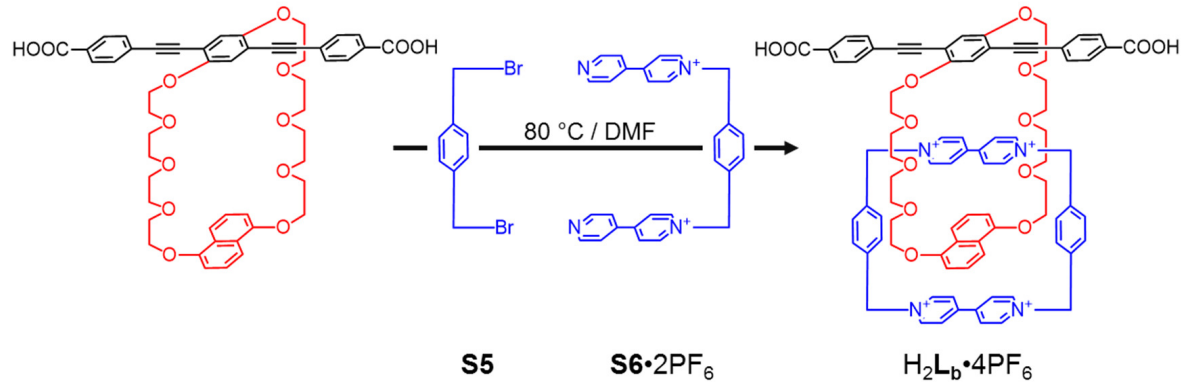

Scheme S4. Synthesis of [2]catenane strut $H_2\mathbf{L_b}$•4PF_6

$H_2\mathbf{L_b}$•4PF_6: A mixture of $H_2\mathbf{L_r}$ (518 mg, 0.592 mmol), **S5** (750 mg, 2.84 mmol), **S6**•2PF_6[S1] (2.08 g, 2.95 mmol), and DMF (50 mL) was heated at 80 °C for 1 h. After cooling the reaction mixture to room temperature, the precipitates were removed by filtration. The filtrate was evaporated by pressure and purified by column chromatography on silica gel using a 7:2:1 (v/v/v) mixture of MeOH / NH_4Cl (2M) / $MeNO_2$ to yield a red product, which was dissolved in H_2O and subjected to counterion exchange to yield $H_2\mathbf{L_b}$•4PF_6 (975 mg, 83%) as a red solid. The spectroscopic data matched that reported in the literature.[S1]

MOF-2000: The standard synthetic procedure for the preparation of MOF-2000 is described in the Methods Summary section. Reactions of various ratios of $H_2\mathbf{L_r}$ and $H_2\mathbf{L_b}$•4PF_6 in the starting solution were prepared by following the same procedure. The total amount of $H_2\mathbf{L_r}$ and $H_2\mathbf{L_b}$•4PF_6 organic struts was kept at 2.74 × 10^{-3} mmol and the relative ratios of the two organic linkers $H_2\mathbf{L_r}$ and $H_2\mathbf{L_b}$•4PF_6 were varied from 8:1, 6:1, 4:1, 2:1, 1:1, 1:2, 1:4, 1:6 to 1:8, in turn. All reactions except the ones with $H_2\mathbf{L_r}$ and $H_2\mathbf{L_b}$•4PF_6 in 1:6 and 1:8 ratios yielded single crystalline MOF samples for analysis.

The crystallization condition reported here is optimized. In addition to DMF, different solvents including MeCN, DMSO and mixed-solvent systems were also tried. In most cases, we obtained polycrystalline or amorphous materials were obtained. Experimentally, the choice of counter anion is mainly limited by the solubility of the corresponding salt of the [2]catenane. For example the chloride or bromide salt of $H_2\mathbf{L_b}$ is water-soluble but does not dissolve in polar organic solvents; while the hexafluorophosphate salt is soluble in organic solvents mentioned above but not in aqueous solutions.

Bromine-Labeled Br-MOF-2000: The synthetic procedure employed here was identical to the MOF-2000 synthesis reported in the Methods Section. Aqueous methylamine solution (Aldrich Chemical Co., 40 wt. % in H_2O, 40 μL) was mixed with anhydrous *N,N′*-dimethylformamide (DMF, EM Science, 2 mL) as a stock solution. $H_2\mathbf{L_r}$-Br_2(1.41 mg, 1.37 μmol), $H_2\mathbf{L_b}$•$4PF_6$ (4.06 mg, 1.37 μmol) and $Zn(NO_3)_2$•$6H_2O$ (EM Science, 5.97 mg, 20 μmol) were dissolved in anhydrous DMF solution (1 mL). The mixture was filtered and injected in a 4-mL vial. After the methylamine stock solution (20 μL) was added, the vial was capped and placed in an isothermal oven at 65 °C for 72 h. Dark red crystals of Br-labeled Br-MOF-2000 were collected and rinsed with DMF (4 × 1.0 mL) after the vial was removed from the oven and cooled to room temperature.

We have considered alterations to the organic struts that would reveal the robustness of MOF-2000 assembly in the face of changing struts. In addition to the Br-labeled $\mathbf{L_r}$ discussed above, other organic linkers similar to $\mathbf{L_r}$ and $\mathbf{L_b}$ were also synthesized. We synthesized derivatives in which (1) the length of the rigid backbone of the struts is longer than those in $\mathbf{L_r}$ and $\mathbf{L_b}$ and (2) one of the charged acceptor components has been substituted by a neutral one. Our preliminary data suggests that even with these changes, we obtain MOF crystals with the MOF-2000 topology. We are now probing the effects of these modifications in more detail.

S1.3 X-Ray Crystallography Characterization

S1.3.1 Single Crystal XRD

A dark red cubic crystal (0.51×0.60×0.60 mm) of MOF-2000, Zn_4O $(C_{50}H_{50}O_{14})_2$ $(C_{86}H_{82}N_4O_{10})$ $(NO_3)_4$, was sealed in a glass capillary and was analyzed using synchrotron X-ray source, revealing a cubic unit cell with $a = b = c = 26.37$ Å. As a consequence of the excess $Zn(NO_3)_2$ utilized during the MOF crystallization, it is expected that the majority of the counterions in the framework are NO_3^- rather than PF_6^- ones. The X-ray intensities were measured at 293 K. All the frames obtained were integrated with the XDS/XSCALE program packages. The integration of the data yielded a total of 6847 reflections to a maximum 2θ value of 34.42° of which 984 were independent and 984 were greater than $2\sigma(I)$. Analysis of

the data showed negligible decay during data collection. Absorption correction was applied by using XDS/XSCALE program packages. The structure was solved by direct methods and the subsequent difference Fourier syntheses and refined with the SHELXTL-97 software package, yielded the cubic space group *Im-3* (No. 204) with $Z = 2$ for the formula based on the elemental analysis. Zn and O atoms in the backbone of the framework were refined anisotropically and all other nonhydrogen atoms were refined isotropically. On account of the flexibility of crown ether and catenated ring, and the free space in the pores of the MOF, the attempts made to model crown ether component residing in the pores of MOF-2000 did not lead to a meaningful identification of atoms belonging to the crown ether. Modeling of electron density within the voids of the frameworks did not lead to identification of all guest entities in structures because of the low resolution of the data. This challenge, which is typical of porous crystals that contain disordered functional groups and solvent filled pores, lies in the raw data where observed strong (high intensity) scattering becomes limited to ~1.2 Å at best, with higher resolution data present but weak (low intensity). In contrast with the common strategy for improving X-ray data collection, increasing the exposure time of the crystal to X-rays did not improve the quality of the high angle data in these cases, as the intensity from low angle data saturated the detector and minimal improvement in the high angle data was achieved. Nonetheless, assignment and refinement of the backbone framework was not unreasonable, as judged by the resulting bond and angle metrics.

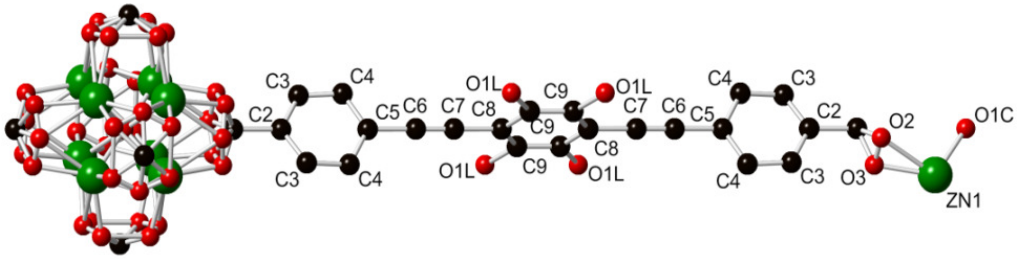

Fig. S1. Ball and stick representation of the asymmetric unit of MOF-2000. Zinc atoms in green, oxygen in red and carbon in black. Here, O1L was presented to label the positions where the crown ether parts were attaching to the framework backbone.

In order to improve the correctness of the atomic positions in the framework the application of the SQUEEZE routine of A. Spek has been performed. Final full matrix least-squares refinement on F^2 converged to $R_1 = 0.1225$ ($I > 2\sigma(I)$) and w$R_2 = 0.3337$ (all data) with GOF = 1.05. Additional details are presented in Table S1. For the structure where the SQUEEZE program has not been employed, final full matrix least-squares refinement on F^2 converged to $R_1 = 0.1806$ ($I > 2\sigma(I)$) and w$R_2 = 0.4686$ (all data) with GOF = 3.931. The empirical formula for crystal structure refinement is $C_{69}H_{24}O_{13}Zn_4$, based only on atoms that could be resolved in the crystal structure, which is in accordance to the MOF-2000 framework backbone. The "SQUEEZE" structure of MOF-2000 has been deposited into the Cambridge Crystallographic Data Centre under deposition number CCDC 968910.

Table S1. Crystal data and structure refinement for MOF-2000

Theoretical formula	$Zn_4O\ (C_{50}H_{50}O_{14})_2 \cdot (C_{86}H_{82}N_4O_{10}) \cdot (NO_3)_4$
Empirical formula	$C_{69}H_{24}O_{13}Zn_4$
Formula weight	1322.36
Temperature	293(2) K
Wavelength	1.00880 Å
Crystal system	Cubic
Space group	*Im-3*
Unit cell dimensions	$a = b = c = 26.370(3)$ Å
	$\alpha = \beta = \gamma = 90.00^\circ$
Volume	18337(6) $Å^3$
Z	2
Crystallographically determined density	0.240 g cm^{-3}
Theoretical density	0.580 g cm^{-3}
Absorption coefficient	0.385 mm^{-1}
F(000)	1324
Crystal size	0.6 × 0.6 × 0.8 mm
2θ range for data collection	12 to 59.6°
Index ranges	$-21 \le h \le 18$, $-20 \le k \le 6$, $-21 \le l \le 21$
Reflections collected	6847
Independent reflections	984[*R*(int) = 0.053]
Completeness to theta = 17.209°	96.4%
Absorption correction	XSCALE
Refinement method	SHELXTL-97
Data / restraints / parameters	984/62/44
Goodness-of-fit on F^2	1.05
Final *R* indices [*I*>2sigma(*I*)]	$R_1 = 0.1225$
R indices (all data)	$R_1 = 0.1322$, $wR_2 = 0.3337$
Largest diff. peak and hole	0.16/−0.24 e. $Å^{-3}$

Based on NMR spectrocopic measurements (Section S1.4) we can determine a theoretical formula for MOF-2000— $Zn_4O\ (C_{50}H_{50}O_{14})_2 \cdot (C_{86}H_{82}N_4O_{10}) \cdot (NO_3)_4$—and therefore, a theoretical density of 0.580 g cm^{-3}. Crystallographically, however, the empirical formula obtained is $C_{69}H_{24}O_{13}Zn_4$, and thus the crystallographically determined density is 0.240 g cm^{-3}, a value which takes into account the SQUEEZE procedure (See Section S1.3.1) which removes disordered electron density from the void space.

S1.3.2 Powder XRD Characterization

Comparison of the experimental PXRD pattern of as-synthesized MOF-2000 (Method Summary) with various input ratios and the simulated MOF-2000 diffraction pattern based on the doubly interpenetrated single crystal structure (red), and the non-interpenetrated structure of MOF-1001[S4] is shown in Fig. S2 and S3. The very high degree of correspondence between the as-synthesized patterns obtained from initial condition L_r:L_b = 1:4 to 4:1(Fig. S3a) with the simulated MOF-2000 diffraction pattern indicates that the bulk materials all have the same double interpenetration as MOF-2000. No extra phase is present amongst the as-synthesized MOF-2000 crystals as evidenced by the fact that there are no extra diffraction peaks which would correspond to the non-interpenetrated form. The experimental PXRD patterns of crystals obtained at 6:1 and 8:1 ratios (Fig. S3b) start to show several extra peaks at 3~4˚ and ~10˚, which are characteristic to the simulated non-interpenetrated MOF-1001 pattern.

In MOF chemistry, bulky organic linkers often result in non-interpenetrated or less interpenetrated frameworks. In this case, while $\mathbf{L_r}$ is less bulky than the $\mathbf{L_b}$ [2]catenane, the crown ether ring attached is still relatively large and bulky enough to avoid interpenetration during MOF formation. We have demonstrated a non-interpenetrated MOF-1002[S4] made purely by $\mathbf{L_r}$ strut. Therefore, the appearance of the non-interpenetrated phase when $\mathbf{L_r}$ ratio increases is not completely unexpected.

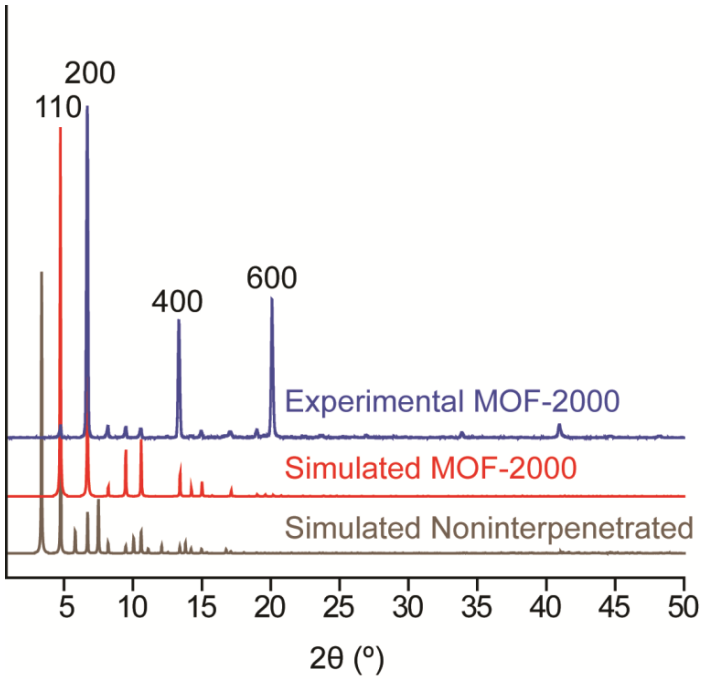

Fig. S2. PXRD comparison. X-ray diffraction pattern (blue) of as-synthesized MOF-2000 crystalline powder compared with the simulated diffraction patterns of two-fold interpenetrated MOF-2000 (red) and non-interpenetrated MOF-1001 (gray).

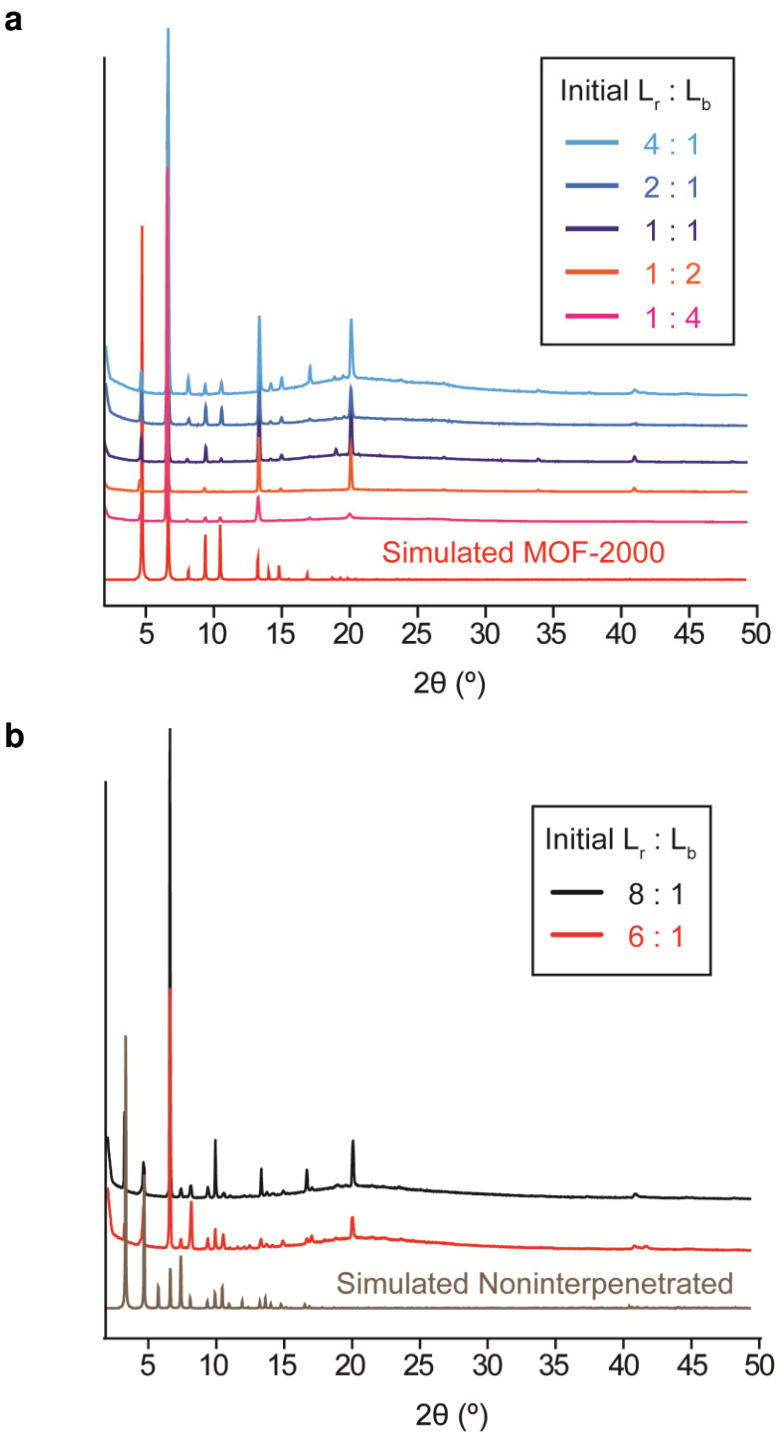

Fig. S3. **PXRD comparison.** PXRD patterns of as-prepared MOF from various initial input ratios compared to the simulated patterns of a) MOF-2000 and b) the analogous non-interpenetrated framework.

S1.4 Nuclear Magnetic Resonance (NMR) Characterization

S1.4.1 Activation Procedures

As-synthesized MOF samples were first immersed in anhydrous DMF for 3 days. During this exchange the anhydrous DMF was refreshed three times a day in order to remove fully unreacted organic compounds and metal salt occluded in the MOF pores. Then the samples were immersed in anhydrous MeCN for another three days, during which time the solvent was decanted and freshly replenished three times a day to fully replace DMF. The solvent-exchanged samples were evacuated with supercritical CO_2 in a Tousimis Samdri PVT-3D critical point dryer. For this step, the MeCN-containing sample was placed in the chamber and MeCN was completely exchanged with liquid CO_2. After this exchange, the chamber containing the sample and liquid CO_2 was heated up around 40 °C and held constant at the supercritical condition (typically 1300 psi) for 1 h. The CO_2 was slowly vented (ca. 8 h) from the chamber at around 40 °C, yielding activated MOF samples.

S1.4.2 Solid State NMR

High-resolution solid-state NMR (SSNMR) spectra were recorded at ambient temperature on a Bruker DSX-300 spectrometer using a standard Bruker magic angle-spinning (MAS) probe with 4 mm (outside diameter) zirconia rotors. Cross-polarisation with MAS (CP/MAS) was used to acquire ^{13}C data at 75.47 MHz. The ^{1}H and ^{13}C ninety-degree pulse widths were both 4 μs. The CP contact time was varied at 1.5 ms and 5 ms. High power two-pulse phase modulation (TPPM) ^{1}H decoupling was applied during data acquisition. The decoupling frequency corresponded to 72 kHz. The MAS sample spinning rate was 10 kHz. Recycle delays for (CP/MAS) between scans varied between 3 and 20 s, depending upon the compound as determined by observing no apparent loss in the ^{13}C signal intensity from one scan to the next. The ^{13}C chemical shifts are given relative to tetramethylsilane as zero ppm, calibrated using the methylene carbon signal of adamantane assigned to 37.77 ppm as a secondary reference.

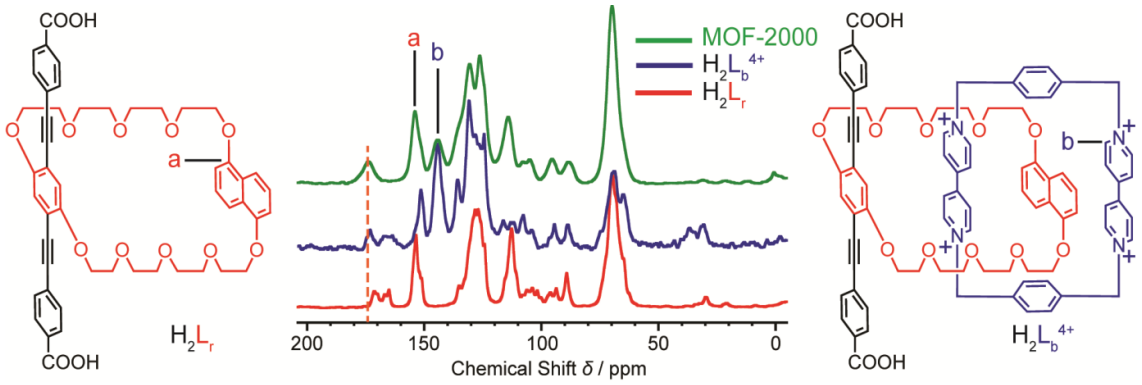

Fig. S4. Solid state ^{13}C NMR spectroscopy. Bulk peaks in the range of 165–171 ppm are observed in organic struts $H_2\mathbf{L_r}$ and $H_2\mathbf{L_b}$•4PF_6 as a consequence of H-bonding interactions between terminal carboxylic groups. In the SSNMR plot of the activated MOF-2000 crystals, the carboxylic carbon peak is shifted to 173.8 ppm, and only one peak is observed, indicating that all the organic links are coordinated to the Zn_4O SBUs and there are no free links trapped in the pores. Both of the finger print peaks from link $\mathbf{L_r}$ (153.1 ppm) and link $\mathbf{L_b}$ (144.2 ppm) are present in the plot of MOF-2000, indicating both links are successfully incorporated into the backbone of the MOF.

S1.4.3 ^{1}H NMR Characterization

To further determine the presence and the ratio of the two organic struts in MOF-2000, single crystalline samples were handpicked from as-synthesized crystals and then activated (see S1.4.1) by supercritical carbon dioxide to remove unreacted struts and solvent molecules that were occluded during the MOF syntheses. ^{13}C CP/MAS NMR Spectrum (see S1.4.2) of the activated sample was taken to confirm that no unbound organic strut is present within the MOF crystals. Activated MOF samples were digested and dissolved with sonication in 1.0 mL dilute DCl solution (prepared from 200 μL of 20% DCl/D_2O solution (Aldrich) and 10 mL CD_3SOCD_3). The digestion solution was used directly for NMR spectroscopy. Proton signals of the ^{1}H-NMR spectrum of acid-digested activated MOF-2000 sample (Fig. S5) can be individually assigned, and the integration of corresponding proton peaks revealed a sharp 2:1 ratio of $\mathbf{L_r}$:$\mathbf{L_b}$ in MOF-2000. Proton a/a' were chosen to determine the ratio is because they are sharp singlets that do not overlap with other peaks. There are a number of dynamic processes in the [2]catenane, such as circumrotation or pirouetting of the macrocycles around each other, that lead to broadened naphthalene and viologen peaks. These considerations, in addition to the inherent ~5% systemic error of typical NMR instruments, lead us to believe that these integrations lie within reasonable range of the expected 2 to 1 ratio.

In order to further investigate the relationship between the population of functionalities in the MOF structure and the organic strut ratio in starting materials, we prepared several reaction mixtures with different molar ratios of $H_2\mathbf{L_r}$ and $H_2\mathbf{L_b}$•$4PF_6$ (from 8:1 to 1:8, see section S1.2) and analyzed all crystal samples obtained in the same fashion. The result is summarized in Fig. 1c. Surprisingly, this 2:1 stoichiometry was found to be consistent and invariant in the $\mathbf{L_r}$:$\mathbf{L_b}$ = 1:4 to 4:1 range.

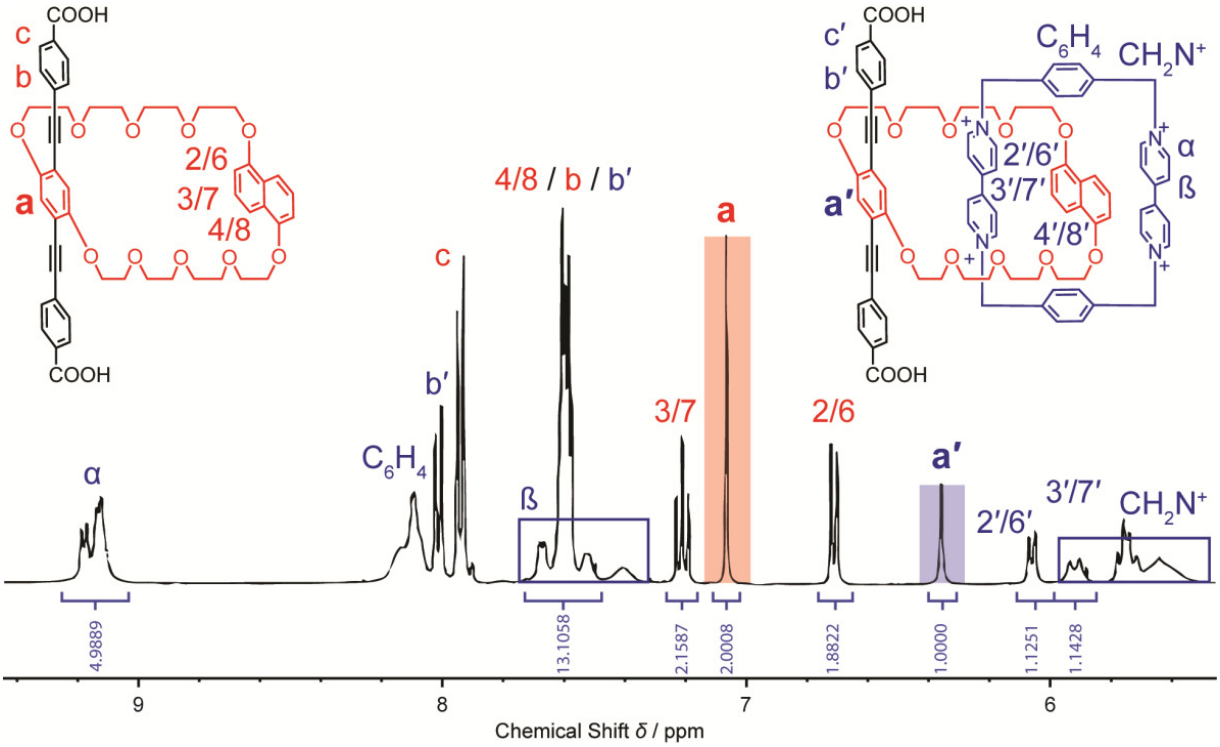

Fig. S5. ^{1}H NMR spectroscopic studies on MOF-2000. Partial ^{1}H-NMR spectra of acid-digested activated MOF-2000 sample prepared from starting solution with a 1:1 ratio of $H_2\mathbf{L_r}$:$H_2\mathbf{L_b}$. The ratio of the two organic struts in MOF-2000 crystal is determined by the integration of proton signals. The accuracy of proton NMR integration is estimated to be ±5%.

S1.5 Optical Characterization (Isotropicity)

The unit cell of MOF-2000 obtained from X-ray crystallography is only defined by the rigid struts and SBUs which effectively contribute to the Braggs reflections. Other than the MOF backbone, X-ray crystallography did not provide further information on the relative positions of the crown ether and [2]catenane subunits as a result of various sources of disorder including: 1) the inherent flexibility of the macrocyclic polyether chains, 2) the chemical bond rotation along the axis of the rigid organic struts, making the crown ether and [2]catenane functionalities point to different directions in the frameworks, 3) the disorder caused by the planar chirality associated with the molecular structures of $\mathbf{L_r}$ and $\mathbf{L_b}$, and 4)

the positional disorder of $\mathbf{L_r}$ and $\mathbf{L_b}$ by the virtue of the same length and connectivity of their rigid struts.

A simple unit cell model of MOF-2000 based on *trans*-$Zn_4O(\mathbf{L_r})_4(\mathbf{L_b})_2$ cluster (Fig. S6a), which may minimize both the steric hindrance caused by the sheer size of the $\mathbf{L_r}$ [2]catenane strut and the electrostatic repulsion associated with its positively charged cyclobis(paraquat-*p*-phenylene) ($CBPQT^{4+}$) subunit is shown in Fig. S6b. The structure corresponds to the 2:1 ordered coloring shown in Fig. 2b. A crystal model (Fig. S6c) was constructed using the *Materials Studio* software package, by employing the *Materials Visualizer* module. It was then geometrically optimized employing the universal forcefield implemented in the *Forcite* module of *Materials Studio*. The atomic coordinates for the inorganic SBUs were obtained from the single crystal X-ray diffraction data, and maintained unaltered during the energy minimization process. This 2:1 ordered structure, where every $\mathbf{L_b}$ [2]catenane strut is aligned along the same axis and surrounded by four $\mathbf{L_r}$ crown ether struts as nearest neighbors, has a perfect 2:1 ratio of $\mathbf{L_r}$:$\mathbf{L_b}$. However, no experimental evidence of anisotropicity was found from optical measurements (Fig. S7 and S8).

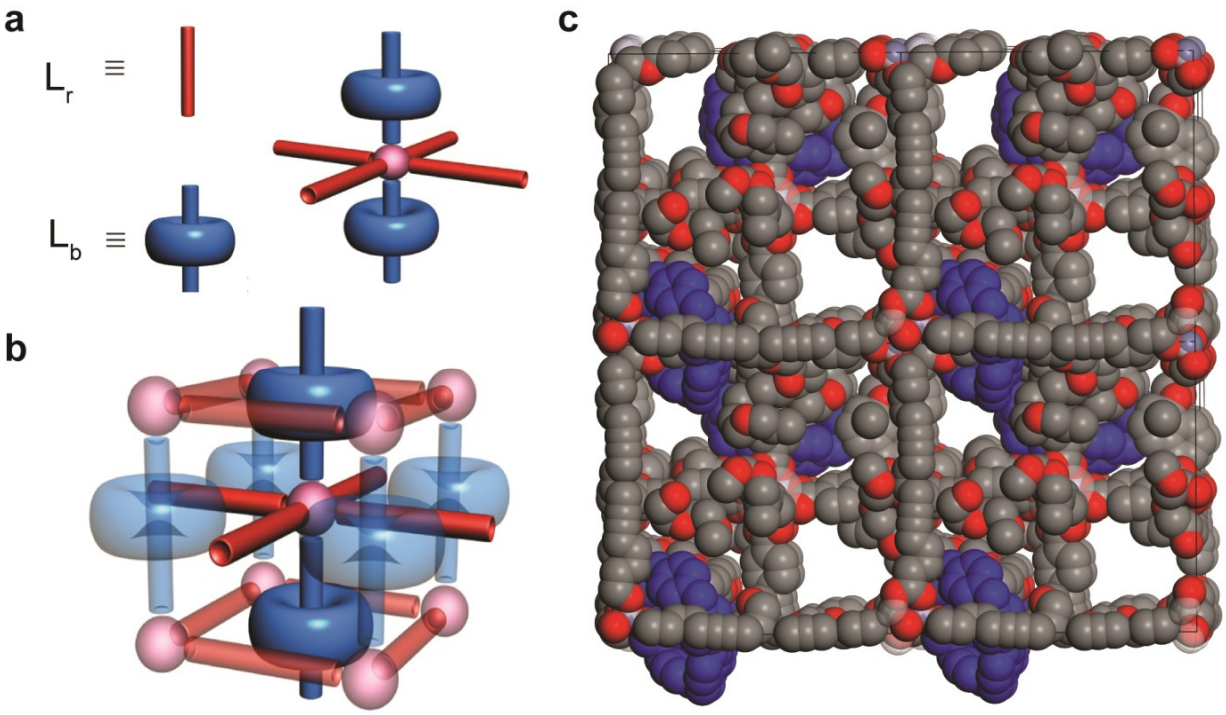

Fig. S6. Materials Studio modeling. Schematic representations of a) the organic struts $\mathbf{L_r}$ and $\mathbf{L_b}$, and the trans-$Zn_4O(\mathbf{L_r})_4(\mathbf{L_b})_2$ cluster, b) the proposed tetragonal unit cell. c) Ball-and-stick representation of a 2×2×2 unit cells model constructed by using Materials Studio software (carbon, black; oxygen, red; Zn, purple; $CBPQT^{4+}$, blue; all hydrogen atoms have been omitted for clarity).

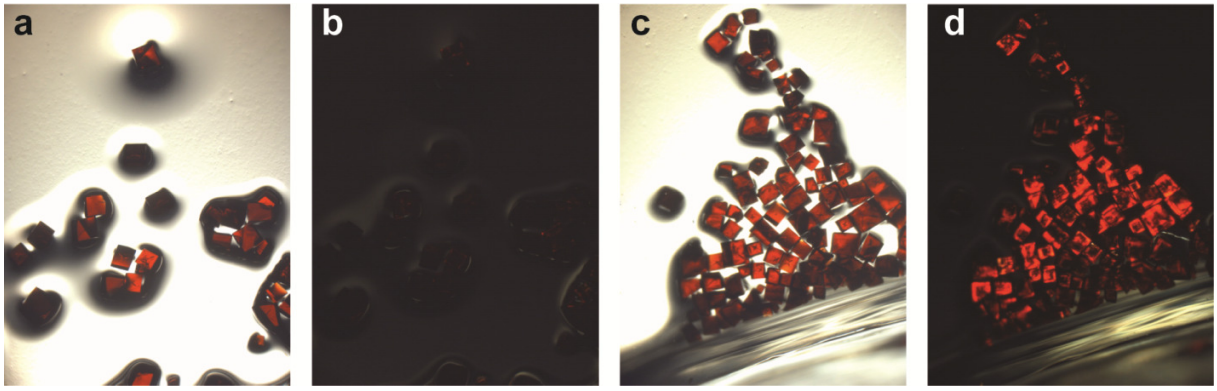

Fig. S7. Polarized optical microscopy. Optical images of as-synthesized MOF-2000 crystals (**a**) in fresh DMF solution, (**b**) in fresh DMF solution placed in between crossed polarizers, (**c**) solvent-exchanged with acetonitrile, and (**d**) solvent-exchanged with acetonitrile, placed in between crossed polarizers. The lack of birefringence in (**b**) suggests that the MOF-2000 crystals are isotropic. Some spots showing weak birefringence can be attributed to defects in the crystals or solvent loss. The birefringence observed in (**d**) is owing to the stress caused by solvent exchange rather than an intrinsic property of crystal symmetry.

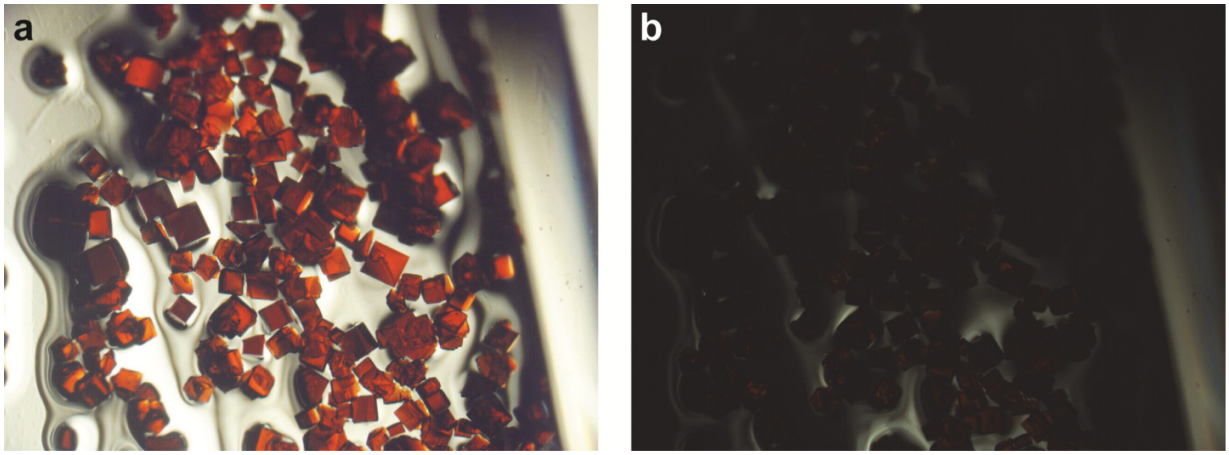

Fig. S8. Polarized optical microscopy of Br-MOF-2000. Optical images of as-synthesized Br-MOF-2000 crystals (**a**) in fresh DMF solution, (**b**) in fresh DMF solution placed in between crossed polarizers. The lack of birefringence in (**b**) suggests that the Br-MOF-2000 crystals are isotropic as well.

S1.6 Thermogravimetric Analysis

Thermal gravimetric analysis (TGA) was performed on both the as-synthesized MOF-2000 and the activated MOF-2000 samples after solvent removal. The experiments were run on a TA Instruments Q-500 series thermal gravimetric analyzer with samples held in platinum pans in a continuous nitrogen flow atmosphere. Samples were heated at a constant rate of 5 °C min^{-1} during all TGA experiments.

In TGA plot of the activated MOF-2000, no weight loss was observed before 200 °C proves complete removal of the guest molecules in the pore. The first weight loss at 200 °C is due to the decomposition of the crown ether and [2]catenane functional groups attached to the backbone of the framework. The second weight loss 350 °C is attributed to the framework destruction. In the TGA plot of as-synthesized MOF-2000, a significant weight loss is observed at relatively low temperate, which can be attribute to the evaporation of solvent molecules inside the pore structure. The other two weight losses are observed at the same temperature of the activated sample.

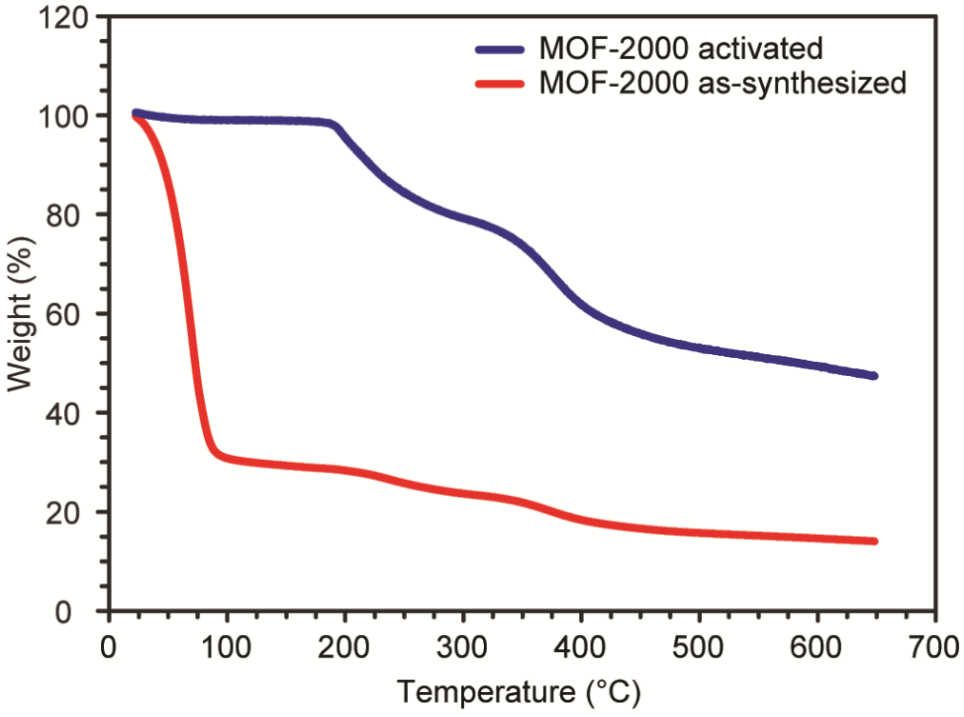

Fig. S9. Thermogravimetric analysis of MOF-2000. Despite its two-fold interpenetration, the MOF-2000 crystal is still highly porous.

Section S2 Additional Simulation Details and Figures

S2.1 Relationship between our Lattice Model of MOF-2000 and the Ising Model

As stated in the main text, our lattice model of MOF-2000, with all nodes colored either blue or red, is equivalent to the Ising model (on a four-connected graph called the **nbo** net). To see this, note that the model interaction energy is such that interactions occur only between nearest-neighbor nodes *i* and *j*, and are of strength $\varepsilon_{C(i)-C(j)}$, where *C(i)* is either *b* (blue) or *r* (red). The Ising model Hamiltonian is

$$E = -J\sum_{i,j}^{edges}\sigma_{C(i)}\sigma_{C(j)} - h\sum_{i}^{nodes}\sigma_{C(i)}\,, \tag{1}$$

where the first sum runs over all distinct nearest-neighbor interactions, and the second sum runs over all nodes. Site *i*'s state or 'spin' is labeled σ_i, and is either +1 or −1. Let blue nodes be spin up (+1) and red nodes be spin down (−1). Then $\varepsilon_{b\text{-}b}$ is the interaction energy between two up spins, $\varepsilon_{b\text{-}r} = \varepsilon_{r\text{-}b}$ is the interaction energy between unlike spins, and $\varepsilon_{r\text{-}r}$ is the interaction energy between two down spins. Evaluating (1) for this set of interactions gives the relations

$$\begin{aligned}\varepsilon_{r-r} - \varepsilon_{b-b} &= E_{--} - E_{++} \\ &= -J + 2\mathrm{h} - \left[-J - 2\mathrm{h}\right] \\ &= 4\mathrm{h}\end{aligned} \tag{2}$$

and

$$\begin{aligned}\varepsilon_{b-r} - \varepsilon_{r-r} &= E_{+-} - E_{--} \\ &= J + h - h - \left[-J + 2\mathrm{h}\right].\end{aligned} \tag{3}$$

From (2) and (3) we have

$$h = \left(\varepsilon_{r-r} - \varepsilon_{b-b}\right)/4 \tag{4}$$

and $$J = \left(\varepsilon_{b-r} - \varepsilon_{r-r}\right)/2 + \left(\varepsilon_{r-r} - \varepsilon_{b-b}\right)/4. \tag{5}$$

Setting $\varepsilon_{r\text{-}r} = 0$ we have finally

$$h = -\varepsilon_{b-b}/4 \tag{6}$$

and

$$J = \frac{\varepsilon_{b-r}}{2} - \frac{\varepsilon_{b-b}}{4}. \tag{7}$$

The simulated 2:1 inherent structures reported in the main text are found in a regime of interaction energies corresponding to an Ising antiferromagnet ($J > 0$) in a nonzero field *h*. Such conditions favor *thermodynamically* a 1:1 composition (at sufficiently low temperature).

S2.2 Additional Simulation Results and Figures

In this section we present results, obtained from our lattice model of MOF-2000, that are intended to supplement the results of the main text. Each figure presented below is called out from the main text, and what follows is a summary of each figure and the conclusion we draw from it.

We first verified that our lattice model of MOF-2000 possesses no thermodynamically stable phase corresponding to a 2:1 red:blue ratio. Figure S10 shows typical trajectories taken from Monte Carlo simulations of the fully-occupied (entirely red or blue) lattice. In these simulations, red-blue interchanges are proposed randomly, and are accepted with the conventional Metropolis rate. These time traces show that the fraction of blue nodes equilibrates rapidly at the conditions simulated, and results in a red:blue ratio that depends on interaction parameters.

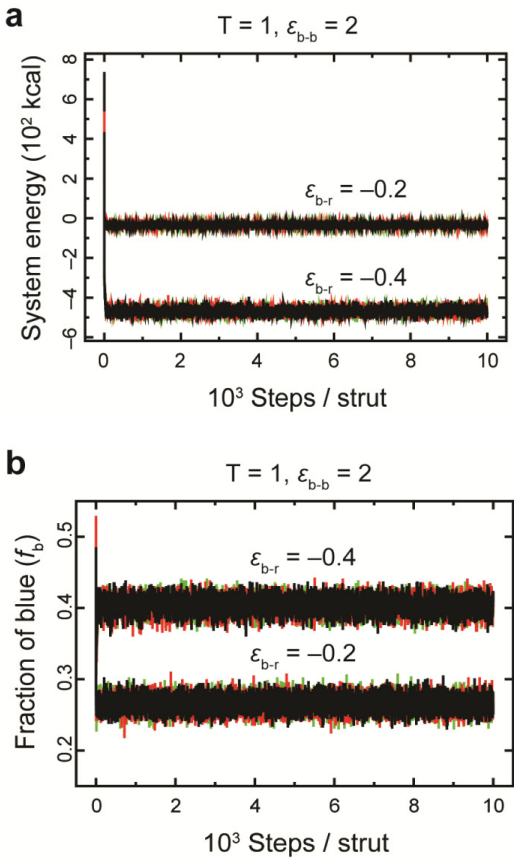

Fig. S10. Example Monte Carlo trajectories. (**a**) For each of the two ($\varepsilon_{b\text{-}b}$, $\varepsilon_{b\text{-}r}$) pairs labeled, three independent simulations (indicated by the red, green and black trajectories) were performed (here $\mu_b = 0$, indicating that red and blue nodes in 'implicit' solution are taken to be equally abundant). Only the first 10^3 steps/node (or 'strut') of the total trajectory (10^6 steps/node) are shown. (**b**) The fraction f_b of the equilibrated system is dependent upon the chosen ($\varepsilon_{b\text{-}b}$, $\varepsilon_{b\text{-}r}$) pair.

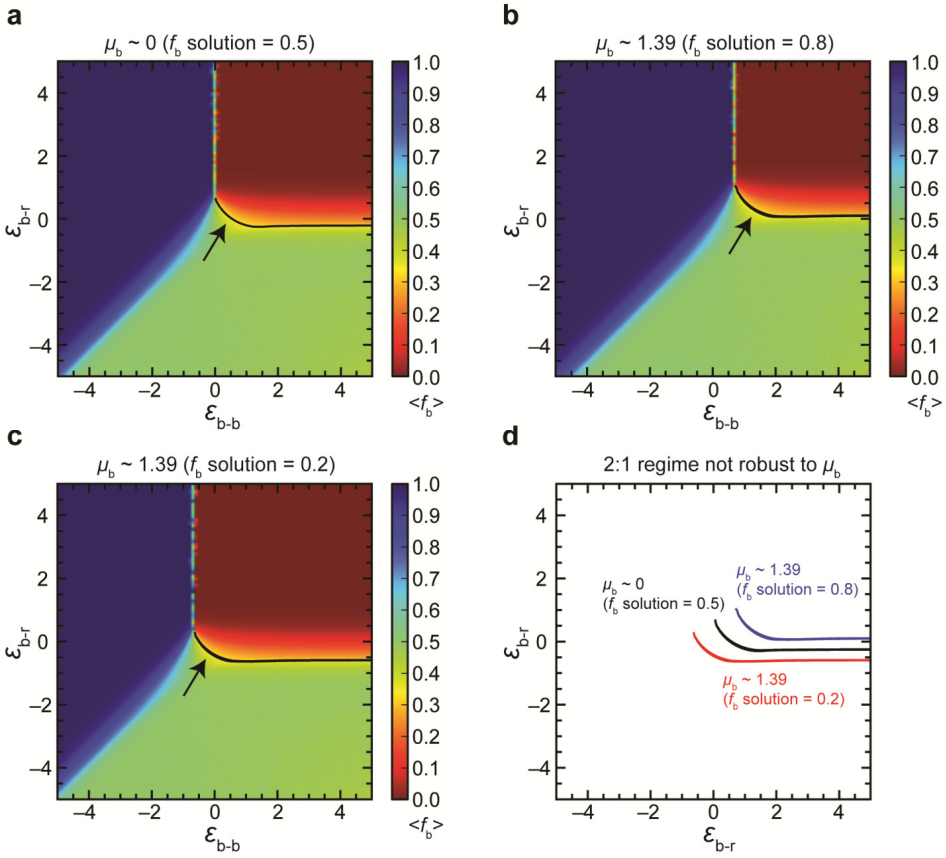

Fig. S11. Equilibrium simulations display no 2:1 red:blue composition regime. (**a-c**) Given a chemical potential μ_b, for each point in ($\varepsilon_{b\text{-}b}$, $\varepsilon_{b\text{-}r}$) space, ten Monte Carlo simulations (of 10^6 Monte Carlo steps per strut) were performed. We show the equilibrium fraction of blue nodes, f_b, in a space of interaction energies ($\varepsilon_{b\text{-}b}$, $\varepsilon_{b\text{-}r}$). (**d**) Although a 2:1 composition is found for certain interaction energies (denoted as lines in **a**, **b** and **c**), no well-defined 2:1 regime exists, and the 2:1 composition is not robust to changes of the red-blue solution composition μ_b.

Figure S11 shows that the red:blue composition obtained from many simulations of the nature described in Fig. S10 shows no extended 2:1 regime, i.e. there is no thermodynamically stable 2:1 "phase" in this model.

There are, however, nonequilibrium configurations possessing a 2:1 red:blue ratio. Figure S12 (**a**) contrasts Monte Carlo simulations done at finite temperature, which equilibrate at a red:blue fraction that depends sensitively on model parameters, with 'inherent structure' simulations. The latter are done in the same way, albeit at zero temperature, and so only node color swaps that do not increase the system's energy are accepted. As shown in panel (**b**), many such simulations 'jam' in configurations whose average red:blue ratio is 2:1.

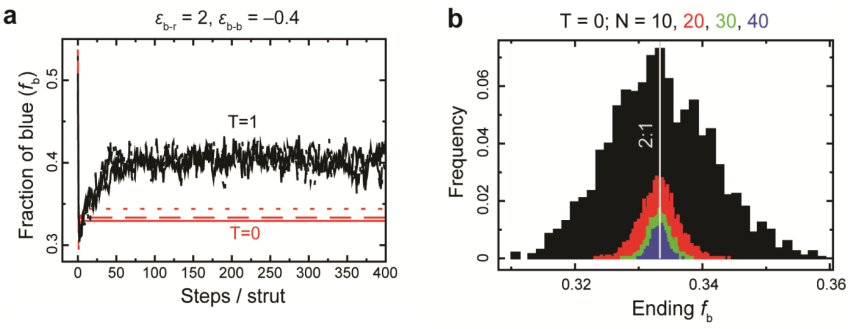

Fig. S12. Equilibrium versus 'inherent structure' simulation trajectories. (**a**) The final fraction of blue nodes obtained from nonzero temperature (equilibrated) simulations are distinct from those obtained from zero temperature (inherent structure) simulations. (**b**) The latter consistently result in structures whose averaged composition corresponds to a 2:1 red:blue node ratio. Results from several system sizes *N* are shown.

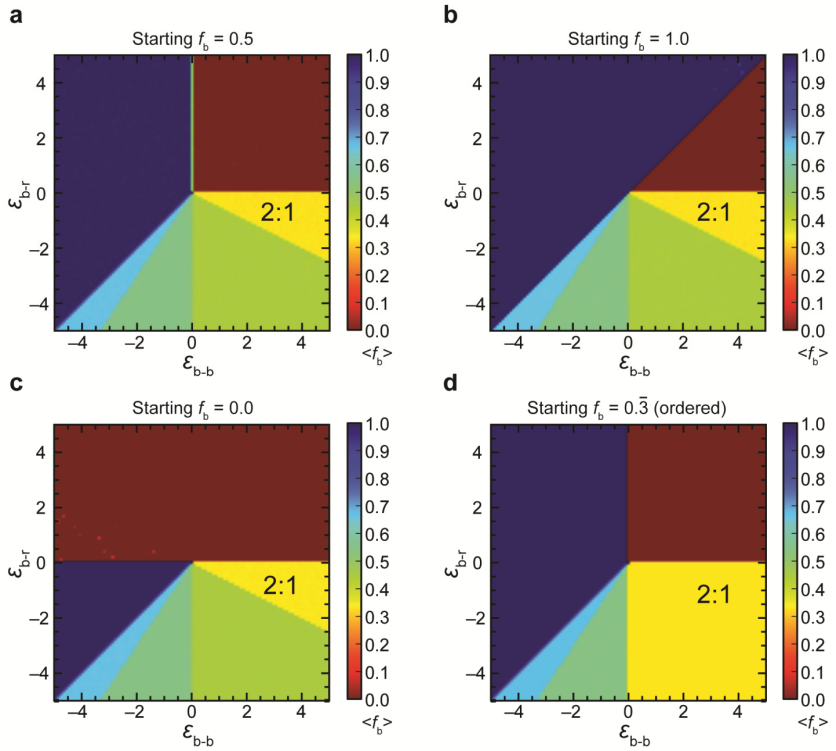

Fig. S13. The out-of-equilibrium 2:1 inherent structure is accessible from a range of initial conditions. Each point on each landscape shown above represents the average of 10 independent zero-temperature color-swap Monte Carlo simulations. Each lattice site was initially colored blue with likelihood f_b (different in each of **a, b**, and **c**), and red otherwise. For reference purposes (**d**) shows results starting from a 2:1 ordered configuration. The presence of the 2:1 regime (yellow) in the regime $\varepsilon_{b\text{-}b} > 0$, $\varepsilon_{b\text{-}r} < 0$, and $|\varepsilon_{b\text{-}r}| < |\varepsilon_{b\text{-}b}|/2$ in each of (**a**–**c**) indicates the existence of a 'basin' of configurations, accessible from a range of initial conditions, that describe, on average, a 2:1 ratio of red:blue nodes.

The zero-temperature or 'inherent structure' analog of Fig. S11 is shown in Fig. S13. This figure shows that 2:1 red:blue inherent structures form in a large regime of parameter space, for a wide range of initial conditions. Taking cuts through this landscape, shown in Figure S14, reveals that transitions between inherent structures with different red:blue ratios are abrupt.

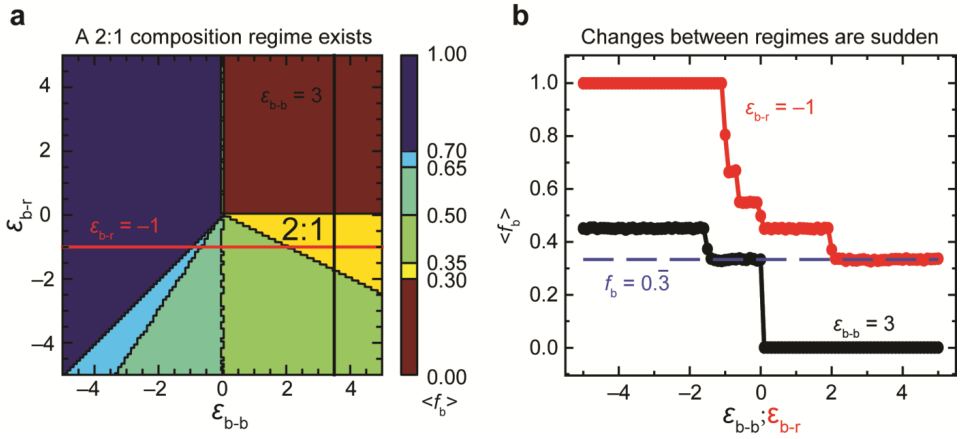

Fig. S14. Transitions between distinct inherent structure composition regimes are sharp. In panel (**b**) we show two "cuts" through the landscape shown in panel (**a**). These cuts reveal that transitions between distinct types of inherent structure occur abruptly with changes of energetic parameters.

We next resolved the spatial characteristics of these inherent structures. Figure S15 describes the local environments (number of red and blue nodes possessed by each node) in three different configurations, each with average 2:1 red:blue ratio. This comparison makes that point that although there exists an ordered 2:1 coloring of the MOF-2000 lattice model, that coloring is strongly anisotropic. The corresponding anisotropy of the experimental system appears to be ruled out by optical investigation (see main text). The 'compositional polycrystal' rendering, shown in panel (**d**), allows one to recognize configurations as a patchwork of 1:1 binary domains. The procedure used to produce these renderings is described graphically in Figure S16.

We note that the description 'compositional polycrystal' is not intended to indicate a rigorous mapping between a conventional polycrystal – a patchwork of crystalline order separated by grain boundaries – and the structures shown. Instead, it is intended to suggest the idea of a patchwork or 'polycrystal' of composition, with 'crystallinity' here taken to mean 'color order' rather than positional order. Regardless of terminology, note that the structures of interest consist of sections of 1:1 red:blue binary order separated by red grain boundaries. For interest's sake, we also show, in Figure S17, two distinct 2:1 structures rendered in terms of the MOF-2000 *physical* framework (i.e. not the virtual sidechain *interaction* framework).

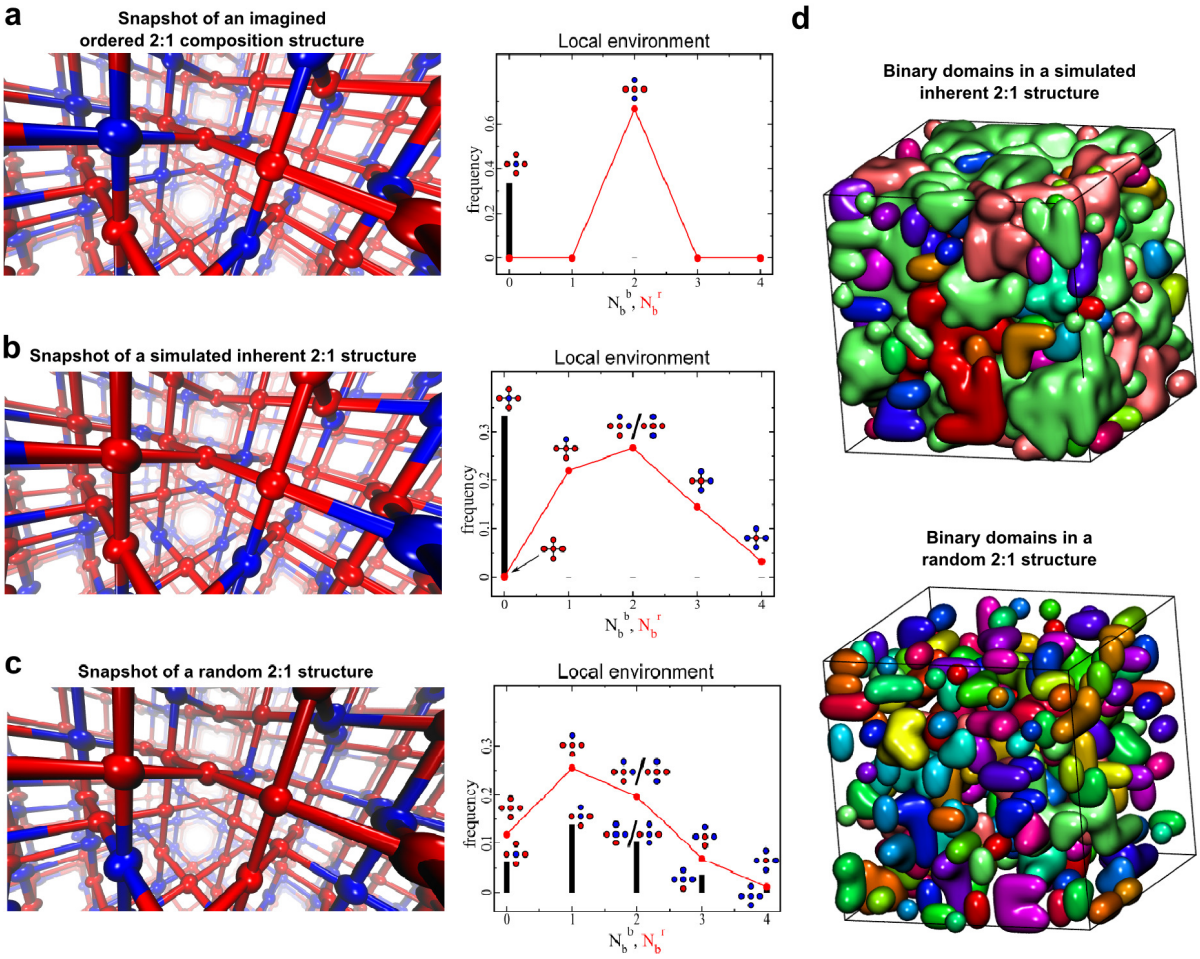

Fig. S15. Comparing imagined ordered, simulated inherent, and random 2:1 structures. The imagined ordered 2:1 structure (**a**) – identical to the theoretical structure described in Fig. 2b – and the 2:1 structure obtained from inherent structure simulations (**b**) display *some* similar properties, i.e., blues are surrounded only by reds, but deviate in the distribution of the types of environments surrounding the red nodes. This difference results in the imagined ordered and simulated inherent 2:1 structures being anisotropic and isotropic, respectively. Additionally, while a random element does exist in the simulated inherent 2:1 structure (**b**), its arrangement differs markedly from a completely random 2:1 structure (**c**), obtained by coloring nodes blue with probability 1/3, and red otherwise. Additionally, large 1:1 domains are present in the simulated inherent 2:1 structure, but not the random one (**d**).

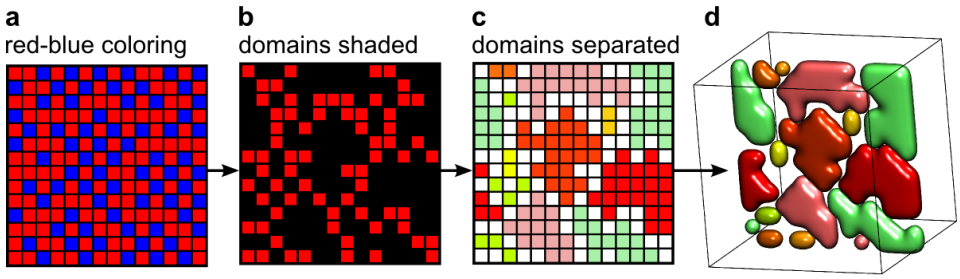

Fig. S16. Identifying and representing individual binary domains. From both local energy minimization (Fig. 3) and growth studies (Fig. 5), the 2:1 regime in MOF-2000 is characterized by a patchwork of 1:1 red:blue binary domains. This patchwork may be more easily visualized in the corresponding 2D square lattice configuration shown above (**a**). Here we show a series of transformations of the configurations shown in (**a**) that first identity (**b**) and then color distinctly (**c, d**) separate 1:1 domains. These domains are separated by all-red grain boundaries. Grain boundaries are shown as red blocks in (**b**), white blocks in (**c**), and white spaces in (**d**).

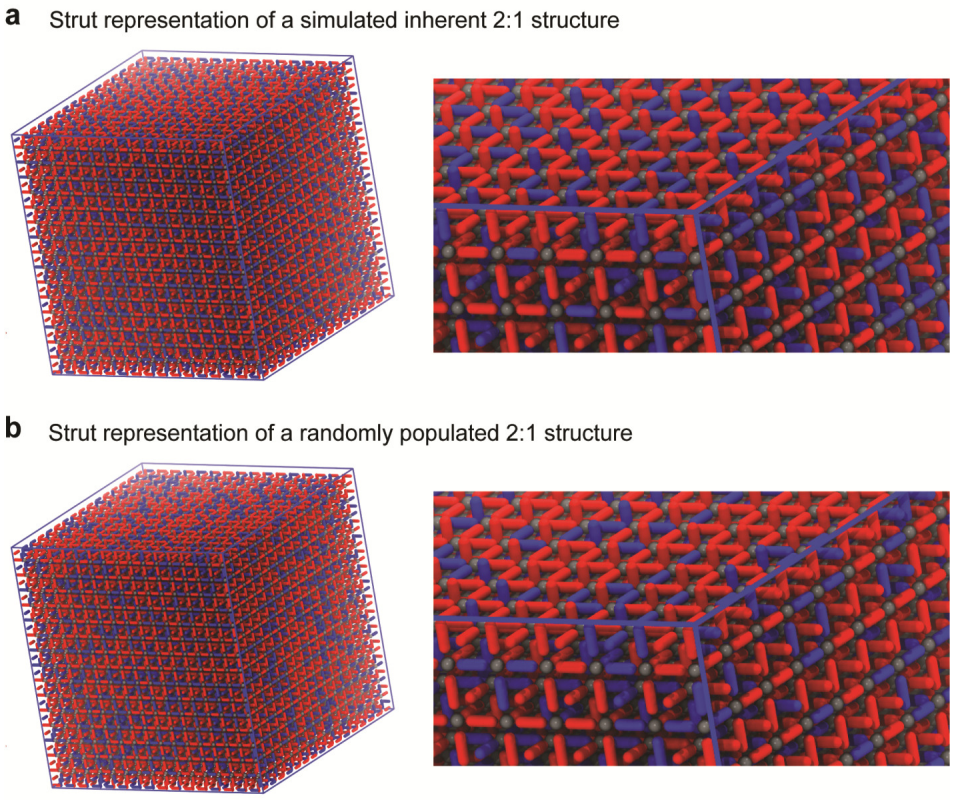

Fig. S17. Renderings of simulation snapshots in terms of the MOF-2000 physical framework. The red and blue nodes in the simulated graphs corresponding to $\mathbf{L_r}$ and $\mathbf{L_b}$ struts, respectively, and are depicted as red and blue pillars. The gray spheres represent the Zn_4O metal clusters. Note that the difference between these structures is much less clear in this representation than in the representation of Fig. S15 (**d**).

The precise numerical values of the red:blue ratios found in inherent structures depend on the topology of the framework. Figure S18 shows that inherent structure simulations done using a 2D square lattice do not show a 2:1 regime. The 2D square lattice shares the *local* four-fold connectivity of the MOF-2000 interaction network; we therefore conclude that *nonlocal* connectivity influences the precise numerical value of the red:blue ratios characteristic of inherent structures.

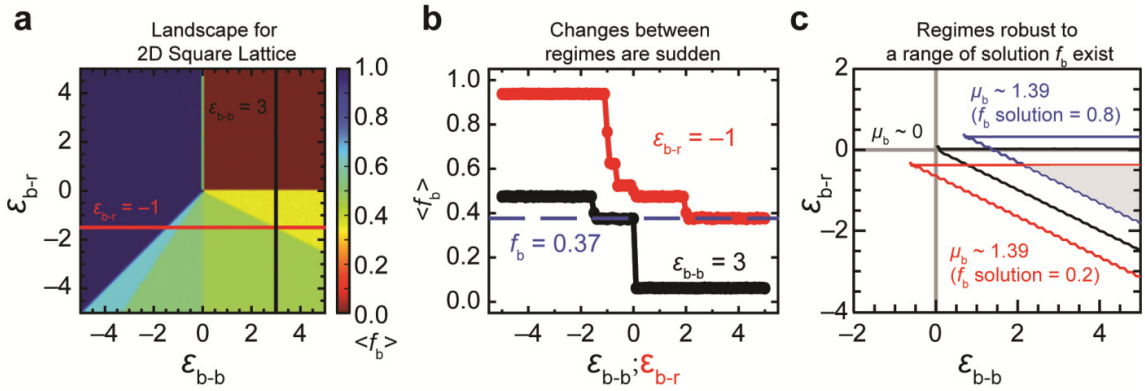

Fig. S18. Inherent structure simulations done on a 2D square lattice do not show a 2:1 regime. The results shown here are similar to the 3D MOF-2000 model (Fig. S14), exhibiting marked transitions between regimes within the landscape (**b**) and robustness to changing solution concentrations (**c**). Despite this similarity, no 2:1 regime exists; the closest blue fraction is $f_b \sim 0.37$. Thus, the exact numerical values of red:blue ratios found in each regime of energy depend on the *topology* of the graph: both the 2D square lattice and the 3D **nbo** net possess identical *local* connectivities.

We describe the difference in the two frameworks' nonlocal structures in Figure S19. This figure shows the graph or net associated with the MOF-2000 lattice model interaction network, and with the 2D square lattice. Although similar at the level of local connectivity, these two lattices differ markedly as one considers connections beyond nearest-neighbor ones. Note that the inherent structure "magic number" ratios are also sensitive to framework topology in higher dimensions. Figure S20 shows the red:blue ratios associated with inherent structures obtained using different networks in d dimensions. All are different numerically, emphasizing that network topology plays a role in determining this ratio.

Figure S21 summarizes in a compact manner the differences in inherent structure composition for the MOF-2000 lattice, the 3D simple cubic lattice (relevant to e.g. MOF-5), and the 2D square lattice: "magic number" ratios are distinct for the distinct frameworks.

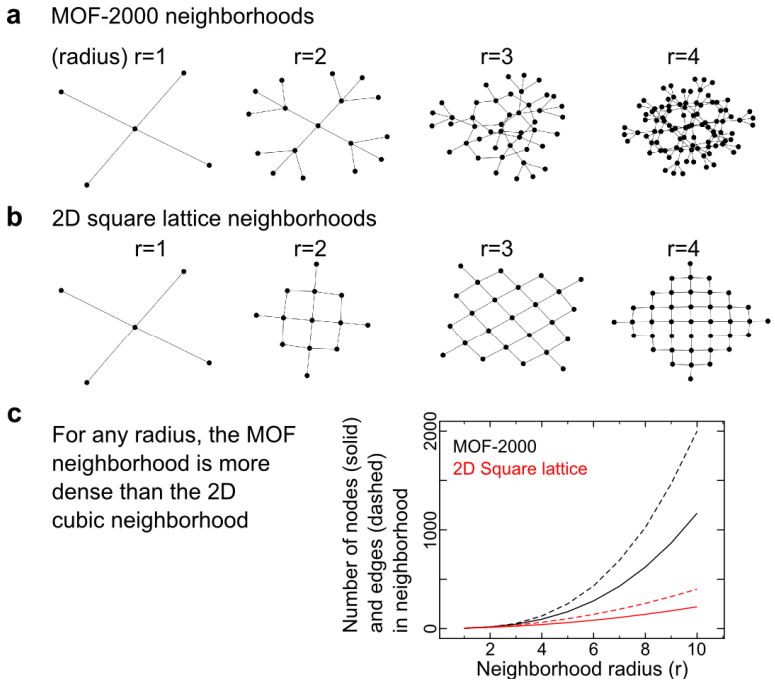

Fig. S19. Global properties of the nbo (MOF-2000 interaction) network and a 2D square lattice. Both networks are locally four-fold coordinated, but are substantially different nonlocally. This distinction is most evident when visualising (**a**,**b**) and plotting the number of interactions (**c**) within a distance *r* from a central node.

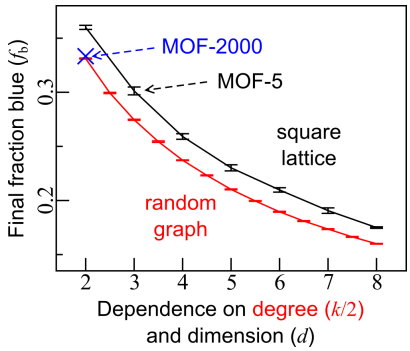

Fig. S20. Different theoretical interaction networks yield distinct magic number ratios. Within the 2:1 interaction regime of MOF-2000 (here we take $\varepsilon_{b\text{-}b}$ = 5, $\varepsilon_{b\text{-}r}$= -0.05), local energy minimization results in configurations with distinct ratios of red:blue for a range of cubic lattices of varying dimension *d* (black curve; 10 simulations per *d*). The factors that determine the magic number ratio are likely nonlocal, given the lack of correspondence in magic number ratios between the cubic lattice graphs and *k*-regular random graphs of identical degree (red curve; 10 simulations per *k*; note that the degree in the square lattice and k-regular graph are 2*d* and the *k*, respectively). Both the square lattices and *k*-regular random graphs were constructed to have at least 10,000 "struts" in size, and were produced using the python network analysis module NetworkX.[S5]

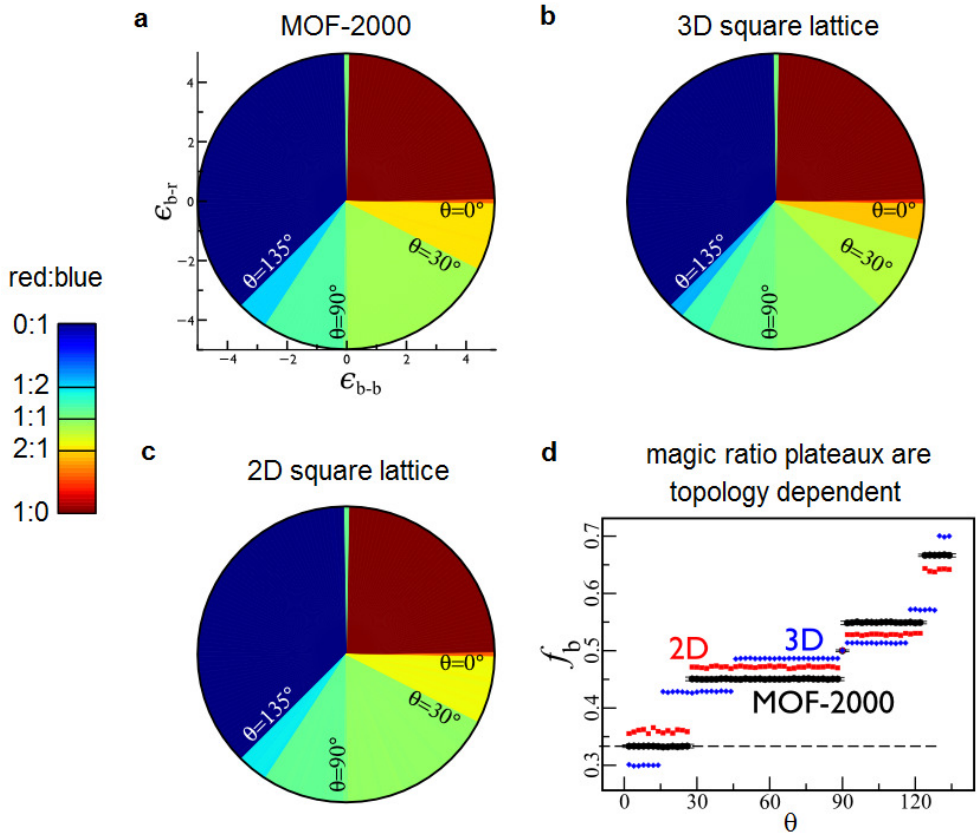

Fig. S21. Inherent structure magic-number ratios exist for each studied interaction framework; their precise numerical values are framework topology dependent. All three topologies shown— **a**) MOF-2000, **b**) the 3D square lattice, and **c**) the 2D square lattice — show discrete magic number ratios in their inherent structure landscapes. These ratios, however, are distinct for the three distinct frameworks, which is evident in the lack of overlap in the plateaux visible for the three topologies (**d**). The plateaux in (**d**) are taken for a circular "slice" of the inherent structure landscape.

We turn finally to the growth simulations described in the main text. Figure S22 shows in cartoon form how red-red binding 'mistakes' can infiltrate regions of 1:1 binary order in growth simulations of the MOF-2000 lattice model. Such mistakes lead to red grain boundaries between regions of binary order. For a range of growth rates, these grain boundaries result in 'compositional polycrystal' configurations very like those seen in inherent structure simulations.

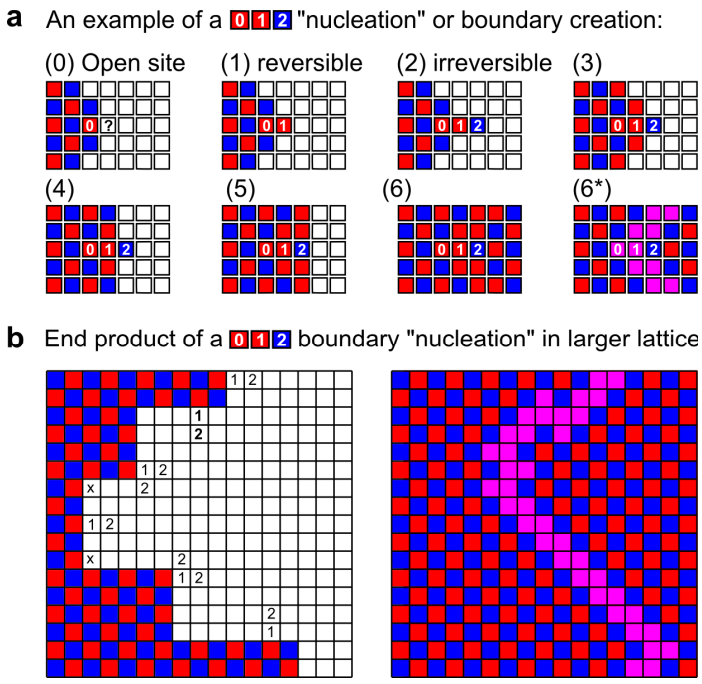

Fig. S22. Cartoon of partially-reversible growth. Illustration of the formation of compositional polycrystal grain boundaries from a series of microscopic binding events: red-red bond "mistakes" are frozen in by the establishment of strong red-blue interactions, and are subsequently propagated as grain boundaries (pink). The resulting red:blue ratio depends on the nonlocal connectivity of the framework, and is 2:1 for MOF-2000.

S2.3 Atomistic Modeling of the 1:1 Binary Arrangement Indicates its Steric Feasibility

We built several molecular models of MOF-2000 in order to establish that a 1:1 ratio of red:blue ($\mathbf{L_r}$:$\mathbf{L_b}$) struts is feasible on steric grounds (i.e. results in no atom-atom clashes). The positions of the strut backbones were obtained from single-crystal diffraction data, and the sidechain ligands were modeled using a previously reported crystal structure of a molecular analogue of the catenane.[S6] In these models, the charge of the ligand is balanced with presence of NO_3^- anions, which is consistent with the synthetic conditions employed to produce MOF-2000.

Geometrical optimizations were carried out using the universal forcefield implemented in the Forcite module of Materials Studio v6.0 to minimize the system's energy and optimize the geometry. Iterations were run until convergence was achieved (convergence criteria being 2.0×10^{-5} kcal mol^{-1} for energy, 0.001 kcal mol^{-1} Å^{-1} for force, and 1.0×10^{-5} Å for atomic displacement). The resulting configurations indicate that the MOF-2000 framework is indeed able to accommodate a 1:1 ligand ratio (see Fig. S23). We also verified that structures with larger $\mathbf{L_b}$, content, e.g. a red:blue ratio of 1:2, are also sterically feasible.

This analysis shows that volume exclusion alone does not immediately suggest particular ratios of sidechains within the framework. As we note in the main text, however, we cannot rule out a thermodynamic origin for the 2:1 ratio seen in experiments; we have instead identified a possible nonequilibrium origin for this ratio.

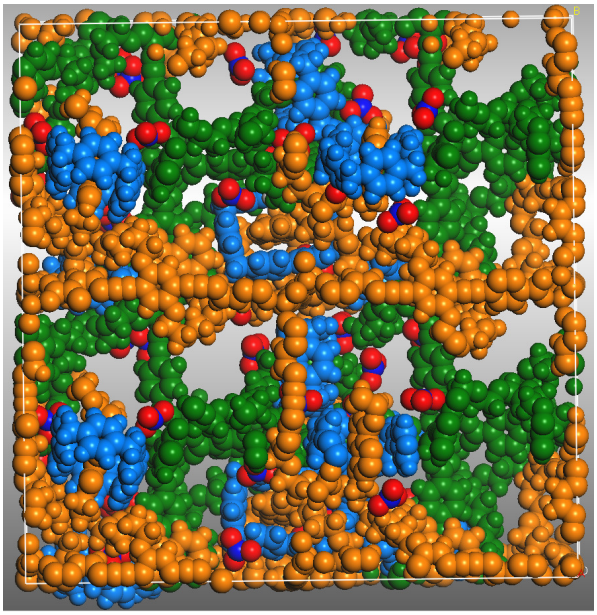

Fig. S23. Molecular model of a framework with 1:1 ligand ratio. The two interpenetrated frameworks of MOF-2000 are shown in orange and green. Light blue are the catenane sidechains arising from each $\mathbf{L_b}$ strut. Nitrate anions (N, dark blue; O, red) are also included to compensate the charges of $\mathbf{L_b}$.

References

S1. Zhao Y-L, et al. (2009) Rigid-strut-containing crown ethers and [2]catenanes for incorporation into metal-organic frameworks. *Chem Eur J* 13:13356–13380.

S2. Fahrenbach AC, et al. (2012) Rapid thermally assisted donor–acceptor catenation. *Chem Commun* 48:9141–9143.

S3. Naoe S, et al. (2012) Gold(I)-catalyzed regioselective inter-/intramolecular addition cascade of di- and triynes for direct construction of substituted naphthalenes. *J Org Chem* 77:4907–4916.

S4. Li Q, et al. (2009) Docking in metal-organic frameworks. *Science* 325: 855–859.

S5. Hagberg AA, Schult DA, Swart PJ (2008) Exploring network structure, dynamics, and function using NetworkX. Proceedings of the 7th Python in Science Conference (SciPy2008), eds: Varoquaux G, Vaught T, Millman J, pp. 11–15

S6. Ashton PR, et al. (1991) The self-assembly of a highly ordered [2]catenane. *J Chem Soc Chem Commun* 9:634–639.